



**Michigan
Technological
University**

Michigan Technological University
Digital Commons @ Michigan Tech

Dissertations, Master's Theses and Master's Reports

2022

NUMERICAL DESIGN OF STEERABLE GUIDEWIRES

Onkar Prakash Salunkhe

Michigan Technological University, osalunkh@mtu.edu

Copyright 2022 Onkar Prakash Salunkhe

Recommended Citation

Salunkhe, Onkar Prakash, "NUMERICAL DESIGN OF STEERABLE GUIDEWIRES", Open Access Master's Report, Michigan Technological University, 2022.

<https://doi.org/10.37099/mtu.dc.etr/1352>

Follow this and additional works at: <https://digitalcommons.mtu.edu/etr>



Part of the [Biomechanical Engineering Commons](#)

NUMERICAL DESIGN OF STEERABLE GUIDEWIRES

By

Onkar Salunkhe

A REPORT

Submitted in partial fulfillment of the requirements for the degree of

MASTER OF SCIENCE

In Mechanical Engineering

MICHIGAN TECHNOLOGICAL UNIVERSITY

2022

© 2022 Onkar Salunkhe

This report has been approved in partial fulfillment of the requirements for the Degree of MASTER OF SCIENCE in Mechanical Engineering.

Department of Mechanical Engineering-Engineering Mechanics

Report Co-Advisor: *Dr Parisa Pour Shahid Saeed Abadi*

Report Co-Advisor: *Dr Gregory M Odegard*

Committee Member: *Dr Smitha Rao Hatti*

Department Chair: *Dr William W. Predebon*

Table of Contents

List of Figures	iv
List of Tables	v
Acknowledgements	vi
Abstract	vii
Numerical Design of Steerable Guidewires	viii

List of Figures

Figure 1. Use of guidewire in biomedical procedures[7] ix

Figure 2. Schematic diagram of layered actuators[10] xi

Figure 3. (a) CAD model of Bi-layered actuator design and(b) Finite element mesh with C3D8 elements (c) Contour of U3 with a transverse deflection of 62 microns.... xii

Figure 4. Effect of Non-actuating layer on strains and deflection induced (a) Transverse Displacement (b) Longitudinal Strain..... xii

Figure 5. Effect of variation in the thickness of non-conductive layer on bending..... xiii

Figure 6. Variation in Young’s modulus of non-conductive layer on Log scale (a) Displacement of the free face (b) Stress developed at the interaction of layers .. xiv

Figure 7. (a) Cross-section of beam (b) Forces on the curved beamxv

Figure 8. (a) Bending of the beam with deflection δ at the free end (b) Approximation of the bent beam in circular curvature..... xvi

Figure 9. (a) Schematic diagram of a component of sandwich spring and boundary conditions (b) Actual view of the deflection of 1.1 mm after applying the potential difference xviii

Figure 10. The plot of transverse displacement of free end vs Young’s modulus of the xix

Figure 11. (a) Schematic diagram of component of Sideways spring (b) Actual view of the deflection after applying a potential differencexx

Figure 12. The plot of transverse displacement of free end vs Young’s modulus of the coil for Sideways Springxx

List of Tables

Table 1. Material Properties for Multilayer actuators.....	x
--	---

Acknowledgements

This work was supported by the American Heart Association, USA, grant #17SDG33660925 (P.P.).

The authors would like to acknowledge the Department of Mechanical Engineering-Engineering Mechanics at Michigan Technological University for providing the computational resources for the project.

Abstract

Biomedical devices are an integral part of the medical industry nowadays. With the increase in cases of heart disease, catheterization procedures are becoming more frequent. Small-scale actuators are needed for the guidance of small-scale catheters and guidewires to remote targets in the human body. Numerical modelling is needed to guide the experiments in developing such steerable devices and to optimize their design. Here, we designed small-scale steerable guidewires by first developing bending actuators and then assembling them with guidewires. The actuators use materials with strain response to electric potential in a very low voltage range that is not harmful to the human body. Our work examined the layered strip configuration for the structure of actuators and identified trends to maximize the bending deformations. Using the commercial software Abaqus, we developed a finite element model based on Piezoelectric actuation to simulate various combinations of materials and geometries and to optimize the design of the actuator and the steerable guidewires. We also developed an analytical model for the actuators and showed that the simulation results are in agreement with the analytical model. Parameters like thickness, length, and different geometrical combinations and their effect on bending were compared. This numerical model can be customized for different materials that can be used for designing these actuators in future.

Numerical Design of Steerable Guidewires

Onkar Salunkhe¹, Dr Parisa Abadi¹

¹Department of Mechanical Engineering-Engineering Mechanics

¹Michigan Technological University, Houghton MI 49931 USA

1. Introduction

Dr. Sven Ivar Seldinger is the radiologist who developed the Seldinger Technique to enter the vascular, urological, gastrointestinal, and other systems through needle puncture. In this technique, the blood vessel is punctured by using a needle[1] and a flexible wire is inserted through the needle into the artery and advanced to the appropriate location for operating on the tissue or organ. Once the wire reaches the location, the needle is removed, and the flexible polyethylene tube is guided over the wire to the site. The wire is then taken off, and the operation is performed. The flexible wire is called the guidewire. The polyethylene tube is called the catheter. A guidewire can be defined as the device used to move in complex channels of the body and guide and position the catheter to the required location. A catheter can be defined as a thin tube device advanced to the required location in the body with the help of a guidewire to perform a variety of functions such as allowing drainage of body fluids, administering medicinal fluids, positioning stents in arteries, and many more such operations.

Guidewires are used for insertion of stents to remove blockages in different parts of the body and for catheter studies, vascular pressure monitoring, and vascular surgeries. Guidewires and catheters move and operate in very delicate organs and tissues of the body[2]. This makes it necessary for them to be very flexible and made of biocompatible material that is not harmful to the patient's body. Guidewires advance in a very complex path in the body. The tip of the guidewire needs to reach the precise location. For this, it should bend correctly through the channels. Thus, the guidewire should exhibit an appropriate combination of flexibility and stiffness.

Multiple mechanisms are used for bending these guidewires such as mechanical wire and soft robotics actuators which use pneumatic designs[3-5]. However, they usually have macro-scale size. Small micro-scale actuators are needed for guiding guidewires with smaller sizes to reach very narrow vasculature. Multilayer strip mechanism can be used to achieve bending in such actuators with different geometric combination of materials with small scales such as thin films[6]. This bending is dependent on geometrical combination and material properties like stiffness of actuators, actuator strain response, thickness of the layers, length of the actuators etc. A bilayer combination of actuator and non-actuator is used here to obtain the trends on maximizing the bending.

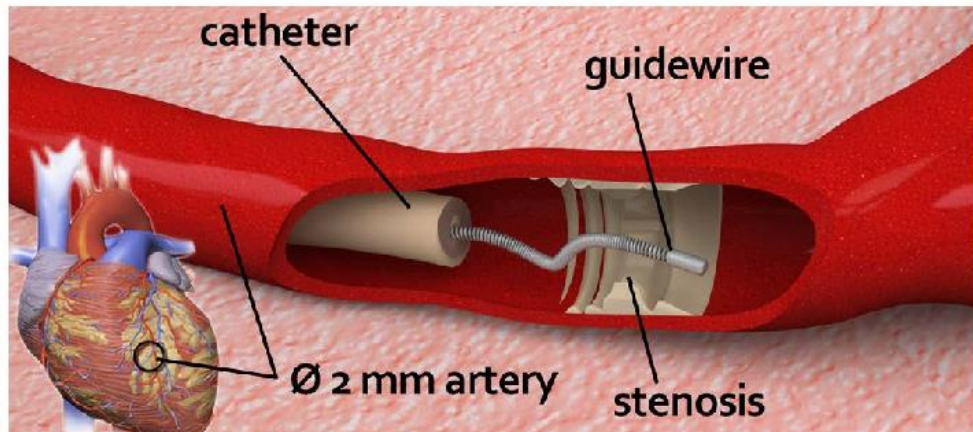


Figure 1. Use of guidewire in biomedical procedures[7]

2. Constitutive model

Here, the goal is to model an electrical actuator, a material that shows strain response to an applied potential difference, including electrothermal and electrochemical actuators. For simulating such a model in a commercial finite element package, the Piezoelectric material model is readily available, and the strain output could resemble the strain developed using other types of electrical actuators as well. Piezoelectric materials show strain response to the voltage or current applied. They show positive strain when positive voltage is applied, and they get contracted when negative voltage is applied[8]. A linear material model was used in this study to reproduce the physical response of voltage applied on the faces. A commercial FE package ABAQUS was used for the simulations.

Generally, actuations in biomedical treatments have low speed. Such procedures include very low strain rates, and thus there are no significant changes in stress and strains which are induced because of dynamics[9]. Hence, the dynamic calculations can be ignored while designing these actuators. We used the ABAQUS standard solver, which is based on stiffness matrix calculations. This eliminated the effect of dynamics in the model and enabled us to solve the model with much lower computational cost.

Piezoelectric formulation based on strain response for the voltage was used for modelling the designs using finite elements. As the strains in the model were not greater than 5%, a linear elastic material model was used[10]. It included Young's modulus and Poisson's ratio as necessary and sufficient constants to run the job. Two important coefficients, the Piezoelectric strain coefficient and the dielectric coefficient (electrical permittivity) were

required. The first one signifies the extent of strain or displacement induced in the element for a potential difference of 1 volt between two surfaces. The second coefficient signifies the extent of polarization of charges in the material. As we were considering only the statics and macroscopic deformation, this wouldn't affect the deformations included, which were of interest to us.

Table 1. Material Properties for Multilayer actuators[11]

Piezoelectric actuator material parameters	
Piezoelectric strain coefficient (m/ohm)	0.1
Dielectric properties-Electrical permittivity (farad/m)	50
Elastic constants	Young's Modulus = 200 MPa, Poisson ratio = 0.3
Non-actuator material parameters	
Elastic constants	Young's Modulus = 200 MPa, Poisson ratio = 0.3

3. Layered actuators

3.1 FE and Material model

The piezoelectric material used in this study is electrically conductive, is biocompatible, and has good mechanical properties. Young's modulus and thickness of actuating layer was kept constant in the initial models. Then, the model was analyzed for bending, with the variations in the Young's Modulus and the thickness of the non-actuating layer.

In the next model, the piezoelectric bending actuator was modelled like a bimetallic strip. This is simple geometry with a rectangular cross-section. The length of the model was kept 5mm referring to commercially available short guidewire tips. Its bending analysis was done theoretically and through ABAQUS simulations. The geometry was analyzed for bending with respect to the thickness and Young's modulus of non-actuating layer.

An FE model for the actuator layer was designed in SIMULIA Abaqus. The cross-section of the actuator layer measured $0.3 \text{ mm} \times 2 \text{ mm}$ ($b \times w$), while the length of the actuator was 20 mm (l) [12,13]. The model meshed with 2 elements along the breadth, 8 elements along the width, and 10 elements along the length. It consisted of a total of 160 elements and 297 nodes. Computational 3-dimensional 8-noded brick elements with piezoelectric response (C3D8E) were used for the actuator elements, while only computational 3-

dimensional 8-noded brick elements with reduced integration (C3D8R) were used for non-actuator material. Only in the case of the actuator layer was the complete model given the properties of piezoelectric material; in the case of both the actuating and the connected non-actuating layer, the width was divided into exactly two halves and assigned the material properties and element type as required. The nodes on the base cross-section were given the boundary condition of encastre (i.e., fixed in all 6 translation and rotational DOFs), and the other cross-section was completely free in all 6 DOFs. A zero-volt potential was applied to the base face, and a 1 Volt potential was applied to the top face of the actuator layer.

Fig. 2(a) represents the schematic diagram of a layered mechanism for bending, while Fig. 2(b) shows the finite element model of the bi-layered mechanism that is studied and discussed in this paper. A CAD model for the actuator layer was designed in SIMULIA Abaqus and studied further. The figure 3(a) shows the two layers in the CAD model while Fig. 3(b) shows the finite element mesh. Fig 3(c) shows the contour plot of bending of the actuator under potential differences. The bending shown is not the actual bending, but rather it is the exaggerated view, as the displacement is in microns. The base face which is fixed and has 0-volt potential is blue, which signifies low displacement, while the top (free) face, which is in red, signifies higher displacement in the Z-axis, which is the transverse direction.

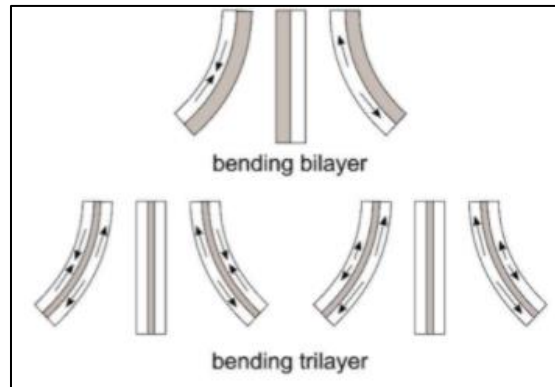


Figure 2. Schematic diagram of layered actuators[10]

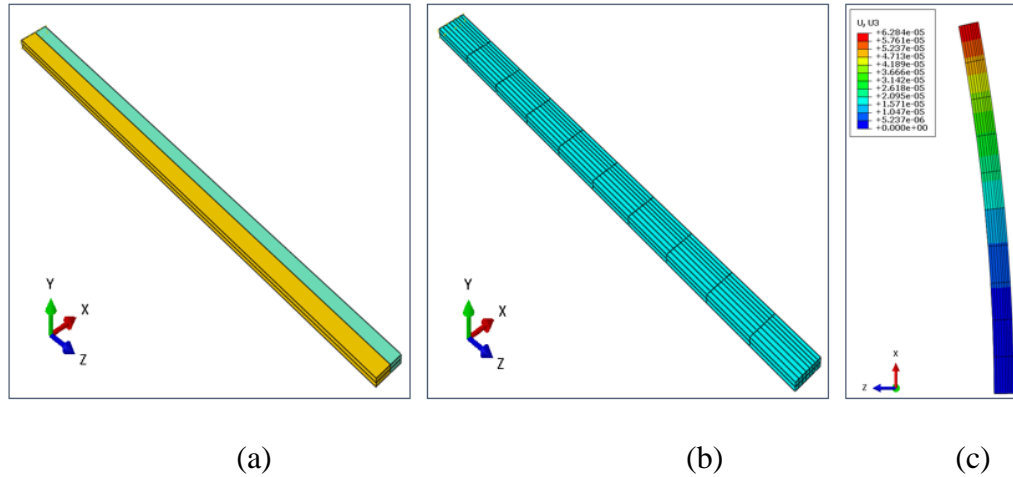


Figure 3. (a) CAD model of Bi-layered actuator design and (b) Finite element mesh with C3D8 elements (c) Contour of U3 with a transverse deflection of 62 microns

3.2 Simulation results

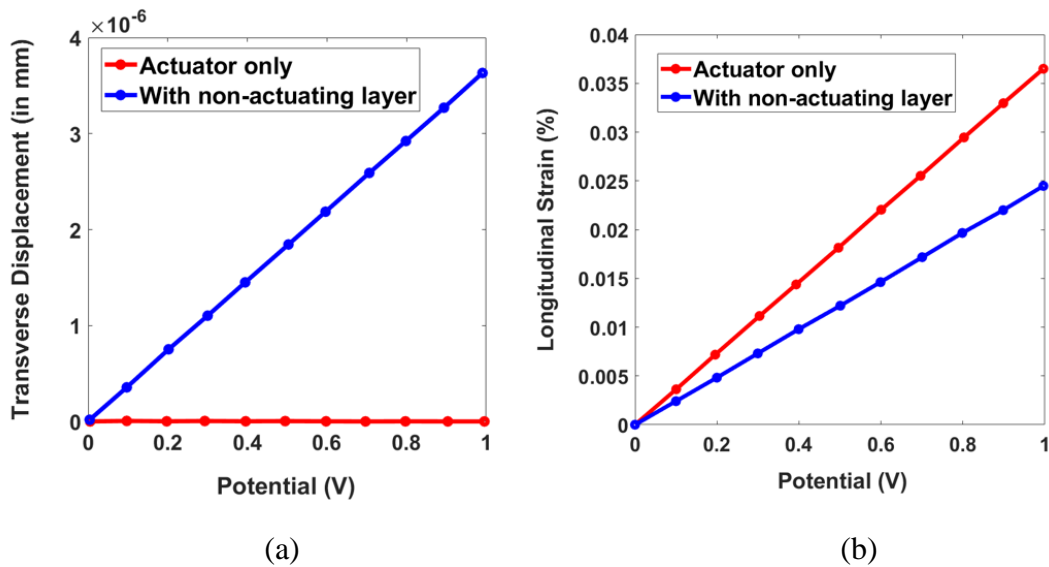


Figure 4. Effect of Non-actuating layer on strains and deflection induced (a) Transverse Displacement (b) Longitudinal Strain

Figure 4(a) shows the comparison of transverse displacement of the top (free) face of the actuator. The displacement is recorded at the mid-point of the cross-section. There was a significant displacement when the non-actuating layer was connected to the actuating layer, which verifies the basic principle behind the bending of the bi-layer mechanism. This transverse displacement is the extent of bending in the actuators. As expected, the variation in the displacement was linear, as we were using the linear material model and strain-

voltage response. As we were observing the displacement in the transverse direction, the longitudinal displacement was getting affected, which can be seen in Fig 4(b). We achieved the bending in the transverse direction with the expense of lower longitudinal strains. So, while designing a bending actuator, we always need to consider this effect when the designer has fixed requirements on axial strain along with transverse displacement.

Multiple simulations were carried out by varying only the thickness of the non-actuating layer, keeping all the other parameters the same. Fig. 5 shows that there is a parabolic trend for the displacement in the transverse direction. The values of thickness ranged from as low as 0.1 mm up to 2 mm. The maximum value of transverse displacement was achieved for the range of 0.5 mm to 1 mm thickness of the non-actuating layer. There was no significant difference in the values of transverse displacement, which was almost the same in all cases.

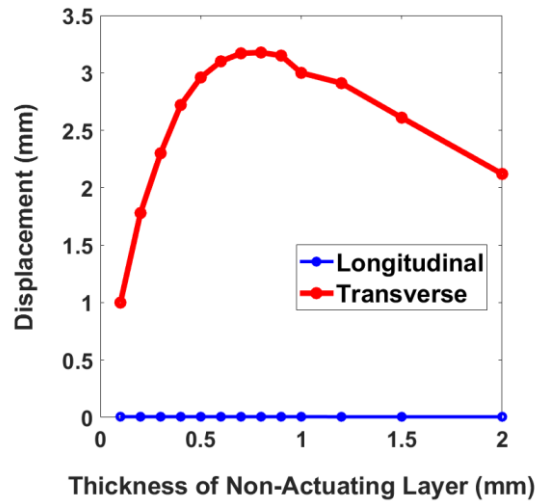


Figure 5. Effect of variation in the thickness of non-conductive layer on bending

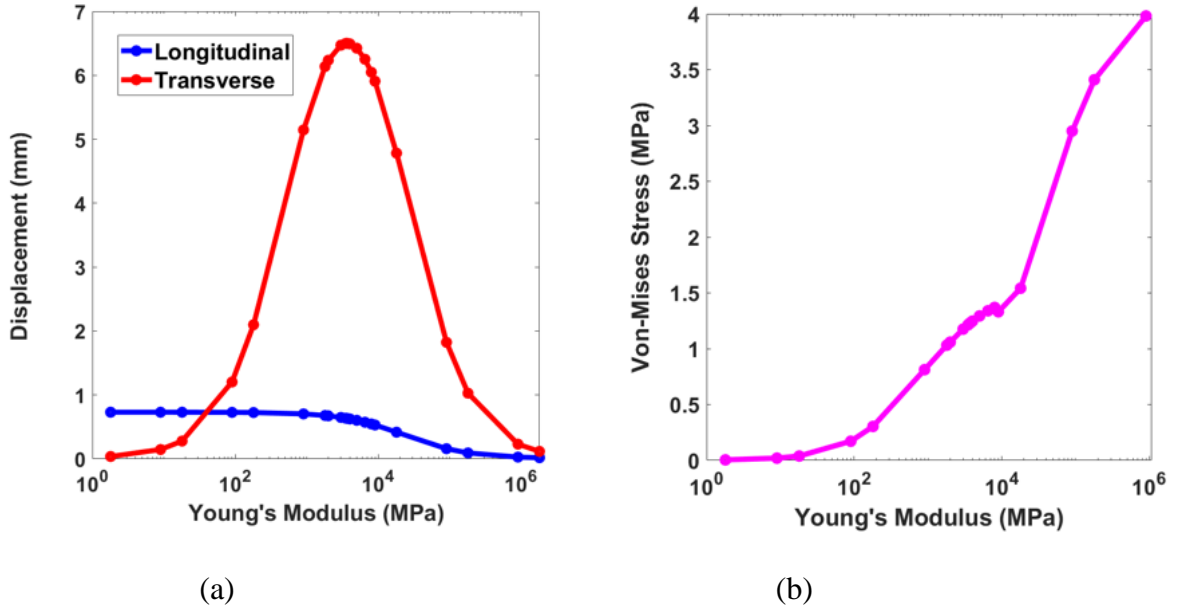


Figure 6. Variation in Young's modulus of non-conductive layer on Log scale (a) Displacement of the free face (b) Stress developed at the interaction of layers

Similarly, the effect of variation of Young's modulus of the non-actuating layer was studied by keeping all the parameters constant and with the thickness of 1 mm for the non-actuating layer. The Young's modulus of actuating layer was 2 GPa; hence, the modulus of the non-actuating layer varied from as low as 1 MPa to as high as 1 TPa. Fig. 6(a) shows the plot with Log scale on the X-axis. Maximum transverse displacement was achieved for the 2 GPa, which is the same as the actuator modulus. This demonstrates that for achieving maximum bending, the modulus of elasticity for both the layers should be in the same range. The bending stiffness is dependent on Young's modulus of the material. This stiffness helps the expanding layer to bend, rather than expand it in axial directions, and achieve the bending of layered actuators.

Interestingly, as we went higher on Young's modulus, beyond the actuator modulus, we found decreased longitudinal displacement, which can be seen in the blue curve in Fig. 6(a). The higher values signify high stiffness, which is not favorable for the benign actuator. Also, very low values of modulus will not give any bending at all. So, to achieve maximum displacement in both transverse and longitudinal directions, the designer should try to keep the modulus of both layers in the same range. The higher values of modulus also increase the stress at the interaction of two layers. In Fig. 6(b), the von-mises stress shows an increasing trend with respect to Young's modulus. Generally, the two layers are joined to each other by precise welding or strong glue to avoid slippage at the interaction. The higher values of the stress are not favorable in the design, as it may lead to slippage or detachment of the layers.

3.3 Analytical model

Along with finite element modelling, a simpler analytical approach was used to verify the simulation results. The deflection of the layered strip was observed to be small in the transverse direction, and also the longitudinal strain was not more than 5%. As the deflection was within the limit, the small-strain theory could be used, which could verify the simulation in a smaller strain range. A layered strip mechanism could be seen, like two thin beams attached to each other with curvature in the middle.

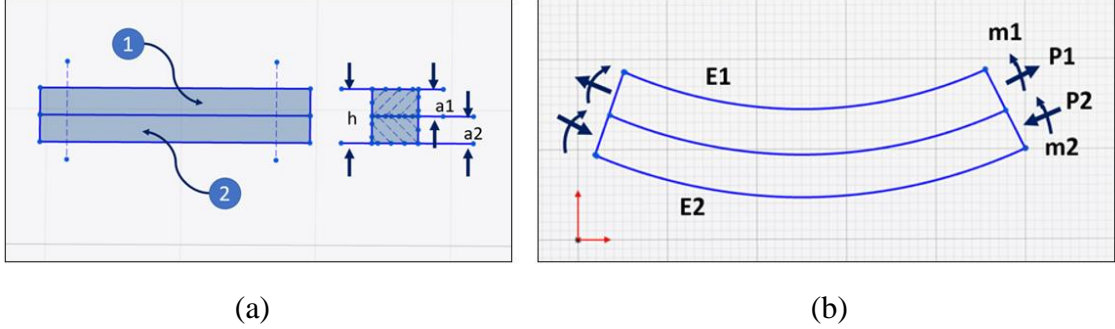


Figure 7. (a) Cross-section of beam (b) Forces on the curved beam

Referring to the Timoshenko method for beam bending[14], consider the two layers of the beam joined to each other as in Fig. 7(a). Assumptions include: 1) the width is very small; it is assumed to be united; 2) contact between the strip is perfectly rigid.; and 3) the cross-section is a plane and remains perpendicular to the curved axis.

E_1, E_2 are Young's modulus of the layers.

a_1, a_2 are the thickness of the layers.

In static conditions, the deformation of the beams is mainly caused by linear expansion, axial loads, and moments. As the deformation of both beams should be equal, we can write the equation:

$$\Delta_1 + \frac{p_1}{E_1 a_1} + \frac{a_1}{2p} = \Delta_2 + \frac{p_2}{E_2 a_2} + \frac{a_2}{2p} \quad \text{eq. (1)}$$

where Δ_1 and Δ_2 are the deformations of the layers individually and ρ is the radius of curvature as shown in Fig 8(a). As the cross-section is equilibrium using force balance, we can assume that $P_1 = P_2 = P$, and using the Flexural rigidity or Euler's equation, we can substitute P , which will lead us to the following equation:

$$\frac{1}{\rho} = \frac{(\Delta_2 - \Delta_1)}{\frac{1}{h} + \frac{2(E_1 I_1 + E_2 I_2)}{h} \times \left(\frac{1}{E_1 a_1} + \frac{1}{E_2 a_2} \right)} \quad \text{eq. (2)}$$

The equation is further simplified to analyze the effect of thickness and Young's modulus.

Let $\frac{a_1}{a_2} = m$, $\frac{E_1}{E_2} = n$ and $I_1 = \frac{a_1^3}{12}$, $I_2 = \frac{a_2^3}{12}$ the equation becomes

$$\frac{1}{\rho} = \frac{6 \times (\Delta_2 - \Delta_1) (1+m)^2}{h(3(1+m)^2 + (1+mn) \times (m^2 + \frac{1}{mn}))} \quad \text{eq. (3)}$$

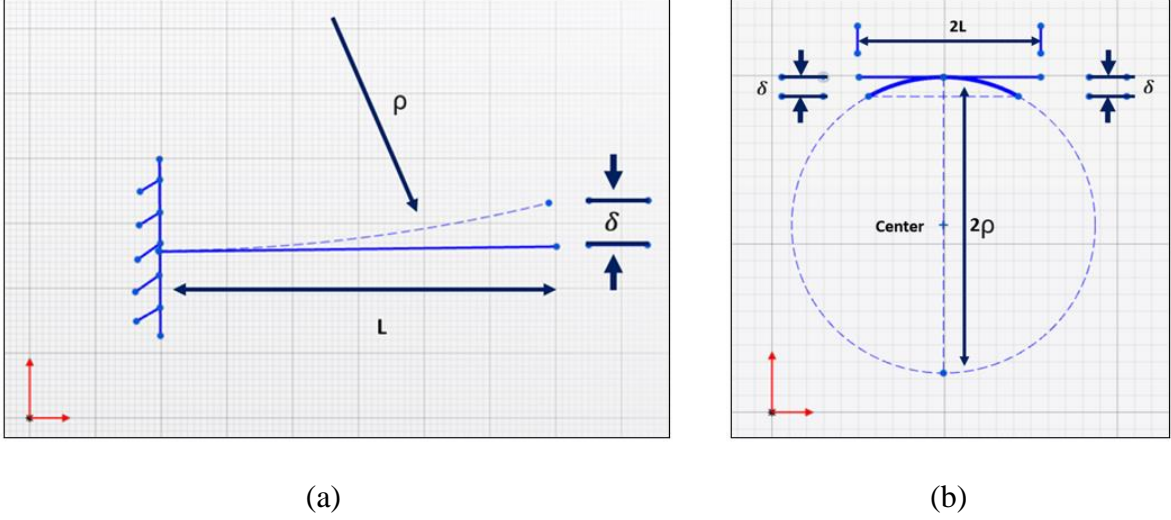


Figure 8. (a) Bending of the beam with deflection δ at the free end (b) Approximation of the bent beam in circular curvature

Similarly, using the standard deflection formula for a cantilever beam under concentrated force at the free end

$$\delta = \frac{PL^3}{3EI}$$

Geometrically, we can calculate the δ in terms of the radius of curvature (ρ), assuming the curvature of the beam is purely circular and has very small deflection. Applying the intersecting chords theorem for the circle in Fig. 8(b),

$$L \times L = (2\rho - \delta) \times \delta$$

$$\delta = \frac{L^2}{2\rho} \quad \text{eq. (4)}$$

Substituting eq. (3) in eq. (4), we get

$$\delta = \frac{3L^2 \times (\Delta)(1+m)^2}{h(3(1+m)^2 + (1+mn) \times (m^2 + \frac{1}{mn}))} \quad \text{eq. (5)}$$

where Δ = Difference in the axial expansion of two layers individually.

As this is a multi-variate expression, the max value of δ can be found by partially differentiating the equations wrt m and n .

$$\frac{\partial(\delta)}{\partial n} = -\frac{n^2}{(n^2+14n+1)^2} = 0 \text{ will give } n = 1$$

Analytically, the maximum deflection can be achieved by keeping the ratio of thickness equal to 1 for small values of deflection.

Putting $n = 1$, and $m = \frac{a_1}{a_2}$ and $h = a_1 + a_2$ in eq. (5)

$$\delta = \frac{3L^2 \times (\Delta)}{a_2} \times \frac{(1+m)}{(3(1+m)^2 + (1+mn) \times (m^2 + \frac{1}{mn}))}$$

Assuming the actuating layer has some constant value unity i.e., $a_2 = 1$ and partially differentiating the above equation wrt m , we get

$$\frac{\partial(\delta)}{\partial m} = \frac{(1-2m)}{(1+m)^4} = 0 \quad \frac{\partial^2(\delta)}{\partial m^2} = \frac{6(m-1)}{(1+m)^5}$$

$\frac{\partial(\delta)}{\partial m} = 0$ will give us $m = \frac{1}{2}$ for maximum deflection

Therefore, we can obtain the max deflection if we keep the thickness of the non-actuating layer half the value of the actuating layer. A similar observation is found in Fig. 5, where the curve is in the maximum region at the 0.6 mm thickness of the non-actuating layer for 1 mm thickness of the actuating layer.

4. Actuator guidewire assembly

To see the effect of geometric combinations of guidewires and actuators, two models were analyzed. The parameters were chosen in such a way that the assembly would give a significant amount of bending, which is necessary for biomedical procedures.

4.1 Sandwich spring

In this geometrical combination, two parallel actuating plates were attached to the non-actuating coil on the periphery[15]. The dimensions of the coil were $r = 50 \text{ microns}$, $R = 175 \text{ micron}$, $l = 5 \text{ mm}$, Pitch = 0.2 mm/revolution. The actuating plates had dimensions of $0.05\text{mm} \times 0.35\text{mm} \times 5 \text{ mm}$. The element type of the plates was C3D8E. As the geometry of the coil was spiral and complex, the tetrahedral mesh with C3D10 elements was used. A piezoelectric strain coefficient and dielectric constant of 1 and 100 were used respectively.

The plates were fixed at one end and assigned zero potential to that end. The other end was free and had different values of potential. The left plate had $-1V$, and the right one had $+1V$.

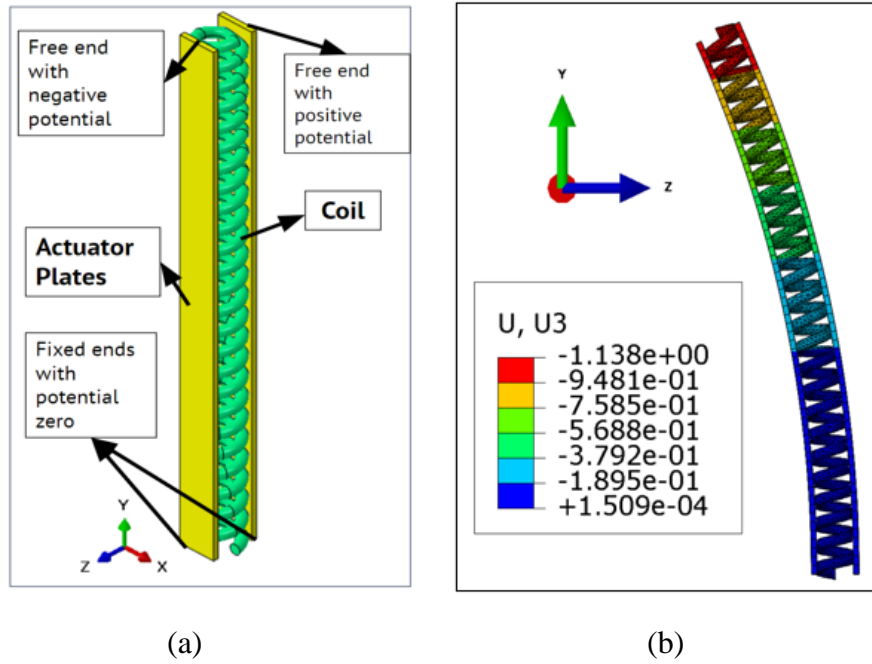


Figure 9. (a) Schematic diagram of a component of sandwich spring and boundary conditions (b) Actual view of the deflection of 1.1 mm after applying the potential difference

The lateral deflection of the model increases linearly with the increase in the piezoelectric coefficient. The dielectric constant should also be increased proportionately to achieve bending. Otherwise, the simulation will abort because of the excessive deformation of the elements.

We investigated the effect of changes in various properties of materials like Young's Modulus of elasticity of plates and coil. The modulus of actuating plates was kept constant, equal to 200 MPa, and the modulus of the coil varied from 10 MPa to 2000 MPa. The coil with 20 MPa showed maximum deflection. This study shows that in the case of sandwich springs, a relatively softer material for the coil shows better bending.

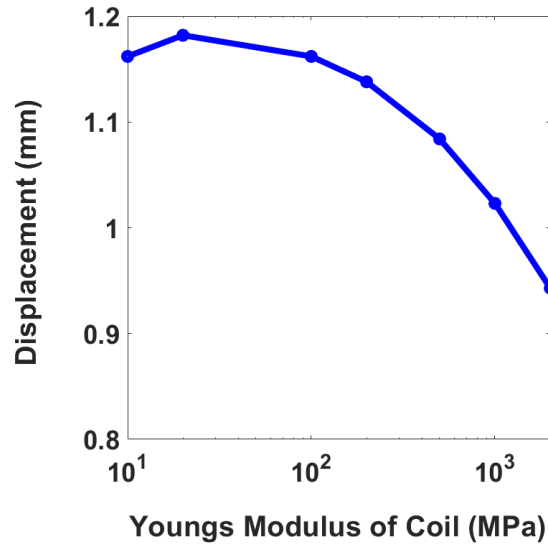


Figure 10. The plot of transverse displacement of free end vs Young's modulus of the

4.2 Actuator plates on one side

Another model was designed in which the piezoelectric actuator was placed on the side of the guidewire, as seen in Fig. 11. The plates had a thin insulator sheet between them. This was used to prevent any electric discharge between the plates having opposite potentials, and the insulator sheet had the same elastic properties as the plates. The material parameters and the dimensions of the coil and the plates were the same as the previous design, while the insulator sheet had a thickness of 0.01mm .

The plates were fixed at the bottom and free at the other end. The plates had zero potential at the fixed end. At the free end, the outer plate (plate no. 1) had positive 1V potential, and the inner plate (plate no. 2) had negative 1V potential.

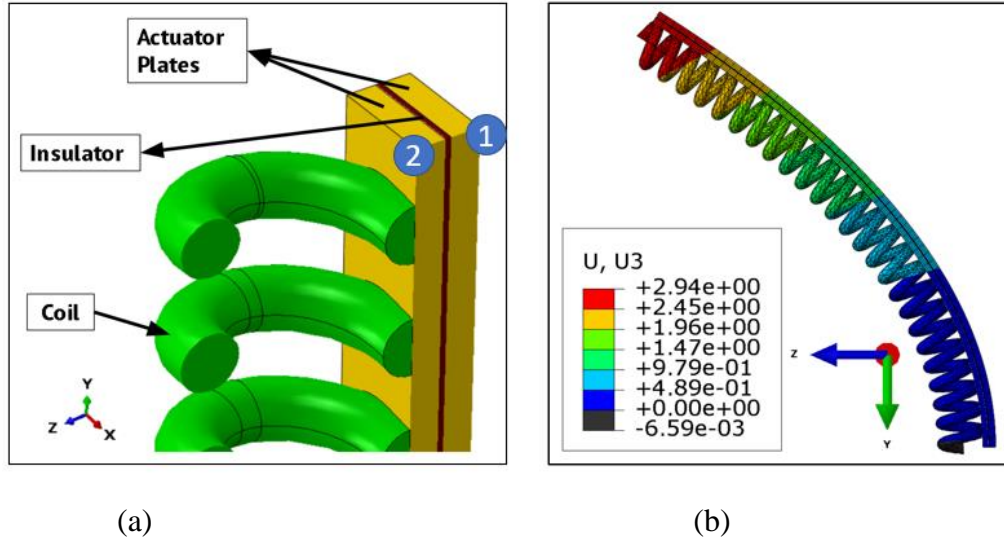


Figure 11. (a) Schematic diagram of component of Sideways spring (b) Actual view of the deflection after applying a potential difference

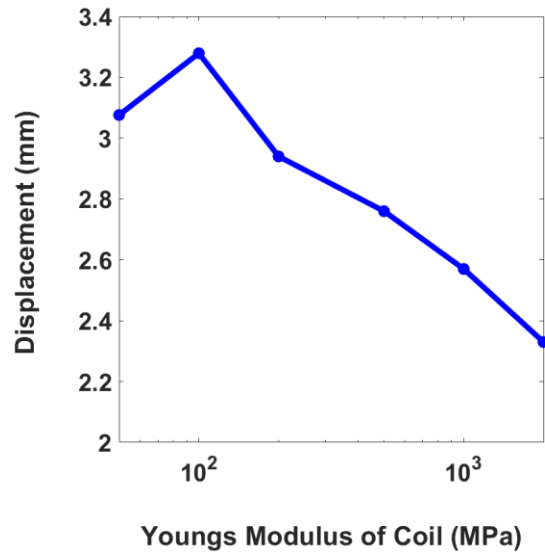


Figure 12. The plot of transverse displacement of free end vs Young's modulus of the coil for Sideways Spring

Like the previous model, this model was studied for variations in Young's modulus of elasticity of coil. The modulus of actuating plates was kept constant, equal to 200 MPa, and the modulus of the coil varied from 50 MPa to 2000 MPa. The coil with 100 MPa showed maximum deflection. This study shows that in the case of sideways springs, the coil with comparably the same Young's modulus exhibits a better bending characteristic.

5. Summary and Conclusion:

A bilayer bending mechanism was investigated for the development of bending actuators for biomedical guidewires. A theoretical study of the same, applicable only for the small strain, was used to validate the results of the commercially available finite element software ABAQUS. The variation of the thickness of the layers for actuating and non-actuating materials was studied, which yielded insight for a better choice of geometry for achieving maximum bending. Similarly, a study of variation of Young's modulus was performed which suggests the two layers in the comparably equal range show better bending characteristics for smaller bending. But for larger bending, where the geometrical nonlinearity is significant, a relatively lower coil modulus shows larger bending. The finite element analysis is very useful when the geometrical nonlinearity is involved, which is very difficult to solve analytically. A computationally effective and simpler finite element model was developed which can be used for analyzing the bending actuators for different materials.

References:

- [1] Ali Awaz, Dick H. Plettenburg, and Paul Breedveld. 2016. "Steerable Catheters in Cardiology: Classifying Steerability and Assessing Future Challenges." *IEEE Transactions on Biomedical Engineering* 63(4):679–93.
- [2] Ali Awaz, Aimee Sakes, Ewout A. Arkenbout, Paul Henselmans, Remi van Starckenburg, Tamas Szili-Torok, and Paul Breedveld. 2019. "Catheter Steering in Interventional Cardiology: Mechanical Analysis and Novel Solution." *Proceedings of the Institution of Mechanical Engineers, Part H: Journal of Engineering in Medicine* 233(12):1207–18. doi: 10.1177/0954411919877709.
- [3] Anon. n.d. "8_BostonScientific_Amplatz Super Stiff™ Guidewire - Boston Scientific."
- [4] Anon. n.d. *Abaqus/CAE User's Manual Abaqus 6.11 Abaqus/CAE User's Manual*.
- [5] Carrell, Tom, Neville Dastur, Richard Salter, and Peter Taylor. 2012. "Use of a Remotely Steerable 'Robotic' Catheter in a Branched Endovascular Aortic Graft." *Journal of Vascular Surgery* 55(1):223–25. doi: 10.1016/j.jvs.2011.07.032.
- [6] Clogenson, H. C. M., A. Simonetto, and J. J. van den Dobbelsteen. 2015. "Design Optimization of a Deflectable Guidewire." *Medical Engineering and Physics* 37(1):138–44. doi: 10.1016/j.medengphy.2014.10.004.
- [7] Ganet, F., M. Q. Le, J. F. Capsal, P. Lermusiaux, L. Petit, A. Millon, and P. J. Cottinet. 2015. "Development of a Smart Guide Wire Using an Electrostrictive Polymer: Option for Steerable Orientation and Force Feedback." *Scientific Reports* 5. doi: 10.1038/srep18593.
- [8] Hu, Xiaohua, Ang Chen, Yigang Luo, Chris Zhang, and Edwin Zhang. 2018. "Steerable Catheters for Minimally Invasive Surgery: A Review and Future Directions." *Computer Assisted Surgery* 23(1):21–41.
- [9] Kruusamäe, Karl, Andres Punning, Alvo Aabloo, and Kinji Asaka. 2015. "Self-Sensing Ionic Polymer Actuators: A Review." *Actuators* 4(1):17–38.
- [10] Luboz, V., Y. Zhang, S. Johnson, Y. Song, C. Kilkenny, C. Hunt, H. Woolnough, S. Guediri, J. Zhai, T. Odetoyinbo, P. Littler, A. Fisher, C. Hughes, N. Chalmers, D. Kessel, P. J. Clough, J. Ward, R. Phillips, T. How, A. Bulpitt, N. W. John, F. Bello, and D. Gould. 2013. "ImaGiNe Seldinger: First Simulator for Seldinger Technique and Angiography Training." *Computer Methods and Programs in Biomedicine* 111(2):419–34. doi: 10.1016/j.cmpb.2013.05.014.
- [11] Meena, K. v., and A. Ravi Sankar. 2021. "Biomedical Catheters with Integrated Miniature Piezoresistive Pressure Sensors: A Review." *IEEE Sensors Journal* 21(9):10241–90. doi: 10.1109/JSEN.2021.3057222.
- [12] Mohd Ghazali, Farah Afiqa, Md Nazibul Hasan, Tariq Rehman, Marwan Nafea, Mohamed Sultan Mohamed Ali, and Kenichi Takahata. 2020. "MEMS Actuators for Biomedical Applications: A Review." *Journal of Micromechanics and Microengineering* 30(7).
- [13] Stoute, Ronald, Marcus C. Louwerse, Jeannet van Rens, Vincent A. Henneken, and Ronald Dekker. 2014. "Optical Data Link Assembly for 360 Mm Diameter IVUS on Guidewire Imaging Devices." Pp. 217–20 in *Proceedings of IEEE Sensors*. Vols. 2014-December. Institute of Electrical and Electronics Engineers Inc.
- [14] Timoshenko, S. n.d. *ANALYSIS OF BI-METAL THERMOSTATS*.
- [15] Tripathi, A. S., B. P. Chattopadhyay, and S. Das. 2019. "Cost-Effective Fabrication of Ionic Polymer Based Artificial Muscles for Catheter-Guidewire Maneuvering Application." *Microsystem Technologies* 25(3):1129–36. doi: 10.1007/s00542-018-4152-3.